Impact of Geogrid Reinforcement on Ballast Performance under Cyclic Loading: A Discrete Element Investigation

Desbrousses, R. & Meguid, M.
McGill University, Montréal, QC, Canada
Bhat, S.
Titan Environmental Containment, Ltd., Iles-des-Chênes, MB, Canada

ABSTRACT
This paper presents the results of a numerical modeling campaign that investigates the microscale interactions and deformation mechanisms of ballast reinforced with geogrids and subjected to cyclic loading. Using the discrete element method (DEM), this study compares the performance of a 300mm-thick unreinforced ballast layer against that of geogrid-reinforced layers, where the geogrid placement depth varies from 50mm to 250mm beneath the tie. The investigation begins with an assessment of the macroscopic behavior of these ballast layers, focusing on the evolution of the tie settlement. The macroscale trends indicate that the tie supported by the unreinforced ballast layer experiences the largest settlement while geogrids positioned within the top 150mm of the ballast layer are the most effective at reducing tie subsidence. Delving into the microscopic response of the ballast is achieved by examining aspects such as the ballast particles' motion, particle contacts, and the energy dissipated through frictional sliding. The simulations reveal that considerable particle movement develops in the upper 150mm of the unreinforced ballast layer characterized by high translational particle velocities. The impact of the geogrid location within the ballast bed on tie settlement is notably distinct, with geogrids located in the top 150mm demonstrating superior effectiveness in reducing tie settlement primarily by restricting particle movement, decreasing the magnitude of inter-particle contact forces, and less energy dissipated through frictional slip.

RÉSUMÉ
Cet article présente les résultats d'une étude paramétrique visant à analyser les interactions microscopiques et les mécanismes de déformation de couches de ballast ferroviaire renforcées par des géogrilles soumises à des charges cycliques. En utilisant la méthode des éléments discrets, cette étude compare le comportement d'une couche de ballast mesurant 300mm d'épaisseur à celui de couches de ballast renforcées par une géogrille ancrée à des profondeurs allant de 50 à 250mm sous les traverses. L'exploration des simulations débute par une analyse du comportement macroscopique des couches de ballast en mettant un accent particulier sur le tassement de la traverse soutenu par le ballast. Les résultats indiquent que la traverse soutenue par la couche de ballast non renforcée subit le plus grand tassement, tandis que les géogrilles positionnées dans les premiers 150mm de la couche sont les plus efficaces pour réduire le tassement des traverses. La réponse microscopique du ballast est examinée en analysant des aspects tels que le mouvement des particules de ballast, les contacts entre les particules, et l'énergie dissipée par le frottement de glissement entre particules. Les simulations révèlent que d'importants mouvements de particules émergent dans les 150mm de la couche de ballast les plus proches de la traverse. L'impact de la position d'ancrage d'une géogrille est important, aves les géogrilles placées dans les premiers 150mm du ballast démontrant une efficacité supérieure dans la réduction du tassement des traverses en réduisant le mouvement des particules, les forces de contacts entre particules, et l'énergie dissipée par glissement de frottement.

1 INTRODUCTION

With close to 49,000km of tracks operated, Canada possesses one of the world's most extensive rail networks (Transport Canada, 2023). The majority of Canadian railroads are supported by ballasted substructures which generally consist of a ballast layer located immediately beneath the ties underlain by a subballast layer itself supported by the subgrade soil (Scanlan, 2018). The ballast layer is typically composed of large angular crushed rocks screened to follow a narrow gradation (D. Li et al., 2015). This assembly of coarse aggregate performs key functions in a railway substructure, including supporting the overlying rail-tie assembly, maintaining satisfactory track alignment, transferring train loads to the underlying soil layers, and providing swift drainage (D. Li et al., 2015; Selig & Waters, 1994). Due to its unbound nature, the ballast layer is prone to deforming substantially under cyclic loading owing to the gradual densification and breakage of its particles coupled with their lateral spread. Deformations in the ballast layer disturb the track alignment by triggering differential tie settlement, with approximately 40% of all track deflections being caused by deformations arising in the ballast layer (Kashani & Hyslip, 2018). Disturbing the track geometry compromises the track riding safety and quality and may lead to train derailment, economic losses, and potential loss of human life. As such, excessive ballast deformations are generally remedied by either imposing speed limits on affected track sections or performing ballast maintenance operations to restore the track alignment. Given that both approaches constitute significant expenses for railroad companies (Chrismer & Davis, 2000), there

exists a need to identify strategies to minimize ballast deformations and curtail the associated maintenance costs.

In recent years, geogrids have increasingly been used to stabilize railroad ballast and improve its in-service performance. Geogrids reinforce ballast by forming a strong mechanical interlock with the granular material, resulting in the formation of a semi-rigid mat that confines ballast particles while allowing geogrids to carry tensile forces ballast aggregate cannot withstand (Jewell et al., 1984). The inclusion of geogrids in railroad ballast has been shown to minimize vertical and lateral ballast deformations, reduce tie settlement, reduce ballast breakage, and increase the substructure's bearing capacity (Das, 2016; Fernandes et al., 2008; Qian et al., 2015; Sharpe et al., 2006). The ability of a geogrid to effectively stabilize railroad ballast and yield optimal reinforcement benefit is contingent on a multitude of factors, including its location within the ballast layer.

The influence of the geogrid placement depth on the behavior of geogrid-reinforced ballast has received considerable research attention. Ballast box tests undertaken by Bathurst and Raymond (1987) on geogrid-reinforced 300mm-thick ballast layers suggested that geogrids located 50mm and 100mm under the ties result in the greatest reductions in tie settlement. However, they recommended using placement depths of 150mm or more to avoid interfering with ballast maintenance operations. Different findings were reported by McDowell and Stickley (2006) after performing ballast box tests on 300mm-thick ballast layers reinforced with geogrids located 100mm and 200mm under the tie. Their work indicated that geogrids placed 200mm under the tie are more effective at curbing tie settlement than those placed 100mm below the tie and cut the need to tamp the ballast layer in half. Experiments on geogrid-reinforced ballast layers conducted by Brown et al. (2007) echoed those findings by suggesting that placing a geogrid 250mm under the tie gives rise to a reduction in tie settlement that exceeds that achieved by a geogrid located 150mm beneath the tie. A discrete element study carried out by Chen et al. (2012) on confined and unconfined ballast box tests revealed that the optimum geogrid placement depth is a function of the degree of confinement to which the ballast layer is exposed. Their results showed that geogrids reduce the movement of ballast particles within a 100mm-thick zone centered at their location and that the optimum geogrid placement depth changes from 100mm to 250mm in the confined and unconfined tests respectively. The effect of the geogrid placement depth on the lateral movement of ballast particles was examined by Indraratna et al. (2013) and Hussaini et al. (2015) who conducted ballast box tests on 325mm-thick ballast layers reinforced with geogrids placed at depths of 130mm, 195mm, 260mm, and 325mm. They reported that embedding a geogrid 195mm under the tie yields the largest reduction in the vertical tie settlement and ballast lateral spread but recommended placing the geogrid 260mm below the tie to avoid interfering with ballast maintenance operations. Additionally, ballast box tests performed on clean and sand-fouled ballast by Sadeghi et al. (2023) suggested that geogrids located 200mm below the tie are more effective at minimizing tie settlement and ballast breakage than geogrids situated at a depth of 100mm.

Given the number of studies that investigated the effect of the geogrid placement depth on the behavior of geogrid-reinforced ballast and the different conclusions drawn from each research endeavor, there exists a pressing need to explore the behavior of geogrid-reinforced ballast and its dependence on the geogrid location from both a macroscopic and microscopic scale. As such, in this paper, the effect of the geogrid placement depth on the behavior of reinforced ballast subjected to cyclic loading is investigated. To do so, a three-dimensional model of ballast box tests performed by Desbrousses et al. (2023) is developed using Itasca's *Particle Flow Code 3D* (*PFC3D*) (Itasca, 2022). Upon calibrating the contact model parameters used in the simulations, 300mm-thick unreinforced and geogrid-reinforced ballast layers are subjected to cyclic loading in which the geogrid placement depth is varied from 50mm to 250mm beneath the tie. The impact of geogrids and their placement depths is then examined by exploring multiple facets of the geogrid-ballast interaction mechanism such as the motion of ballast particles, the transmission of loads in the granular assembly, and energy dissipation.

2 BALLAST BOX TEST SIMULATIONS

2.1 Previous Experimental Work

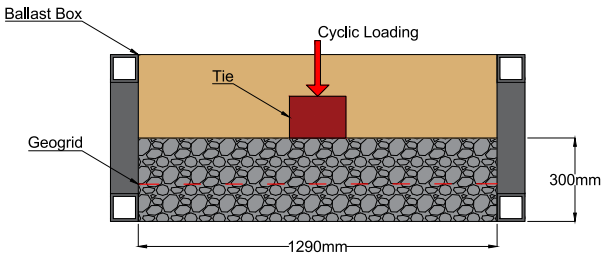

Figure 1. Schematic of the experimental setup used by Desbrousses et al. (2023).

Desbrousses et al. (2023) performed ballast box tests in a container with plan dimensions of 915×1,290mm and a height of 600mm hosting 300mm-thick ballast layers constructed in three 100mm-thick lifts (see Figure 1). The ballast aggregate used in the experiment was screened to conform with an AREMA No. 4 gradation and had a mean diameter (D_{50}) of 27.5mm. Different subgrade strengths were considered in the experiments by lining the bottom of the ballast box with different rubber mats with equivalent California Bearing Ratios (CBR) of 25, 13, and 5. For each support condition, four tests were conducted on unreinforced and geogrid-reinforced ballast layers. In the reinforced case, a single geogrid with dimensions of 700×1,030mm was placed at a depth of either 150, 200, or 250mm beneath the tie. Upon constructing a given ballast layer, a steel tie with plan dimensions of 301×203mm was placed atop the granular layer and subjected to 40,000 load cycles.

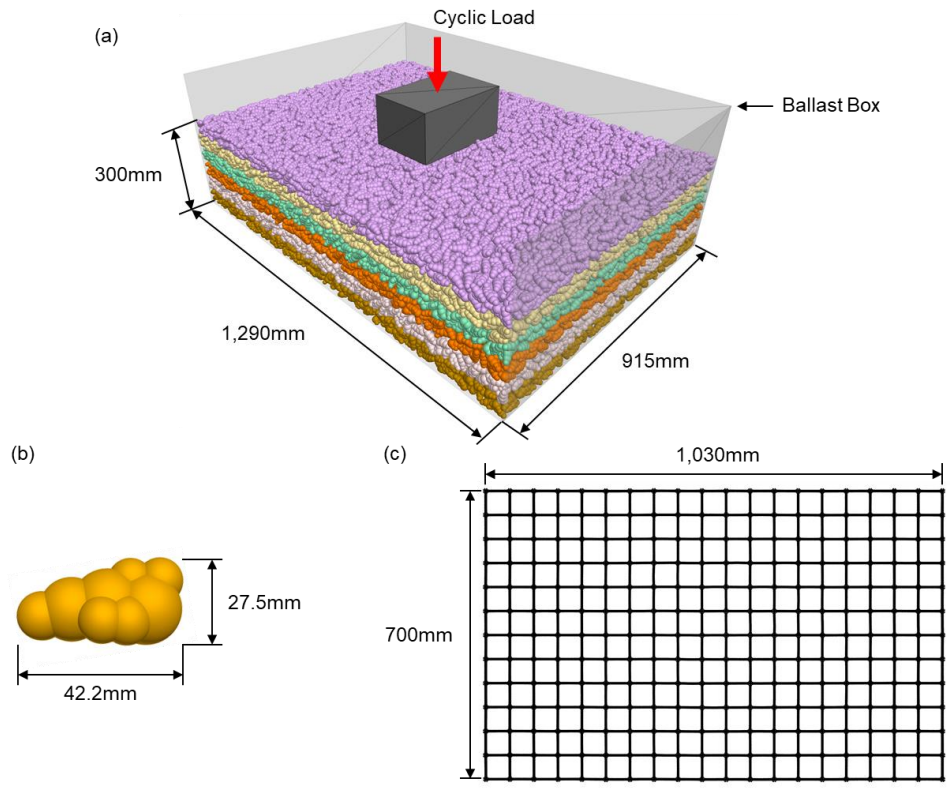

Figure 2. Discrete element model of the (a) ballast box, (b) ballast particle, and (c) biaxial geogrid.

2.2 Modeling Procedure

In the discrete element simulations presented herein, ballast particles are modeled using an eight-ball clump as shown in Figure 2b. The clumps are generated using *PFC3D*'s *BubblePack* algorithm to replicate the shape of a scanned ballast particle with a certain degree of fidelity. Interactions between contacting clumps are governed by the linear contact model. Calibration of the linear contact model's micromechanical parameters is achieved by simulating triaxial tests performed by Suiker et al. (2005) on AREMA No. 4 ballast at confining pressures of 10.3 and 68.9kPa. Using a trial-and-error approach, the linear contact model's effective modulus E^*, the normal-to-shear stiffness ratio κ^*, and friction coefficient μ are varied until the simulation results match the experimental data as depicted in Figure 3a and b, giving an E^* of 325MPa, κ^* of 1, and μ of 0.55.

The large-aperture geogrid used by Desbrousses et al. (2023) in their experiments is modeled as a string of bonded overlapping spheres (Figure 2c) using the linear parallel bond contact model which establishes the presence of a circular interface between contacting pieces capable of carrying both a force and a moment. The micromechanical geogrid parameters are calibrated by following the procedure described by Stahl et al. (2014) in which index laboratory tests such as the multi-rib tensile test and aperture stability modulus test are simulated and compared with experimental data. Given that geogrids embedded in railroad ballast seldom experience strains exceeding 2% in the field (Nimbalkar & Indraratna, 2016), multi-rib tensile tests are simulated up to a maximum strain of 2% and compared with experimental data obtained by Desbrousses et al. (2021) for the geogrid used in their ballast box tests. The aperture stability modulus (ASM) test is simulated following the methodology described in ASTM D7864 and compared with data published by the geogrid's manufacturer (Titan Environmental Containment, 2020). Using a bond effective modulus $\overline{E^*}$ of 465MPa and a bond normal-to-shear stiffness ratio of $\overline{\kappa^*}$ of 1 result in a simulated tensile strength at 2% strain and an ASM of 11.08kN/m and 0.748N.m/deg respectively compared to 11.01kN/m and 0.75N.m/deg obtained experimentally.

The ballast box is simulated in *PFC3D* using facets. The linear contact model is used to describe the interactions between the box's walls and the ballast particles. As recommended by Li & McDowell (2020, 2018), the box's side walls are assigned the same micromechanical contact parameters as the ballast particles. On the other hand, the box's bottom wall is assigned distinct normal and shear stiffnesses (k_n, k_s) of 2×10^5N/m to capture the presence of a soft subgrade with a CBR of 5 beneath the ballast layer. The values of k_n and k_s are obtained by simulating the first twenty load cycles of a ballast box test performed on an unreinforced ballast layer supported by a subgrade with a CBR of 5 as reported by Desbrousses et al. (2023) and shown in Figure 3c.

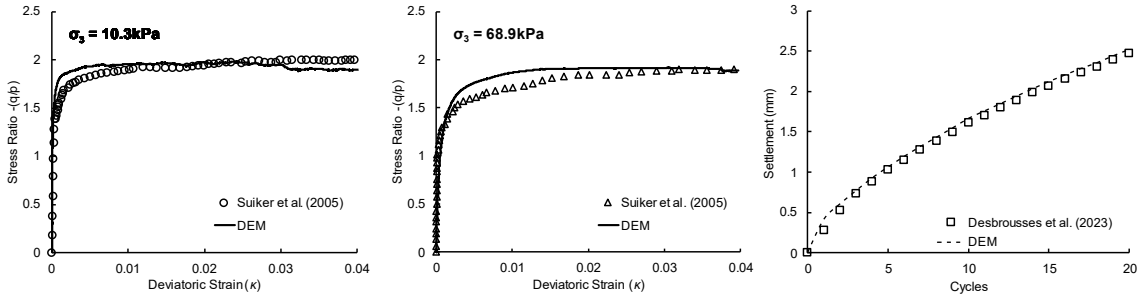

(a) (b) (c)

Figure 3. Discrete element simulations of triaxial tests conducted by Suiker et al. (2005) at confining pressures of (a) 10.3, (b) 68.9, and (c) simulation of the first twenty load cycles on an unreinforced ballast layer supported by a subgrade with a CBR of 5.

The 300mm-thick ballast layers are generated using the Improved Multi-Layer Compaction Method proposed by Lai et al. (2014) in which the ballast assembly is constructed in six 50mm-thick lifts in a gravity-free environment where the friction coefficient is set to zero. When generating a geogrid-reinforced ballast layer, a geogrid is created and embedded in the ballast layer once the ballast genesis process reaches the desired geogrid placement depth. Upon creating the entire ballast layer, gravity is turned on, the friction coefficient is set to its final value, and the model is cycled to equilibrium. A model tie with plan dimensions of 203×301mm is finally placed on top of the granular assembly to receive cyclic loading. Figure 2a depicts a fully completed ballast layer.

2.3 Parametric Study

The goal of this study is to assess the effect of the geogrid placement depth on the response of geogrid-reinforced ballast by delving into the granular assembly's micromechanical behavior. To do so, six ballast box tests are simulated on unreinforced and geogrid-reinforced 300mm-thick ballast layers. In geogrid-reinforced ballast assemblies, a single geogrid sheet measuring 700×1,030mm is embedded at a depth of 50, 100, 150, 200, and 250mm beneath the tie. During each test, a total of twenty load cycles is applied to the tie located atop the ballast layer at a frequency of 10Hz with a mean load of 14kN and a load amplitude of 10.5kN.

3 RESULTS

3.1 Tie Settlement

The simulations are first analyzed by comparing the total tie settlement recorded in each ballast box test as shown in Figure 4. The largest tie settlement of 9.8mm occurs in the unreinforced ballast layer following the application of twenty load cycles. The introduction of geogrids into the ballast layers results in a reduction of the tie settlement, with the extent of this reduction being dependent on the geogrid's placement depth. Specifically, tie settlements of 7.5mm and 7.8mm are recorded in ballast assemblies reinforced with geogrids positioned at depths of 250mm and 200mm respectively. These values represent decreases of 23.4% and 20.4% in tie settlement compared to the unreinforced ballast layer. A marked enhancement in the reduction of tie settlement produced by geogrids transpires at geogrid placement depths of 150mm or less. Geogrids located 150mm, 100mm, and 50mm beneath the tie gives rise to tie settlements of 5.1mm, 4.9mm, and 4.8mm respectively, constituting an average reduction in tie settlement of 49.5% compared to the unreinforced scenario.

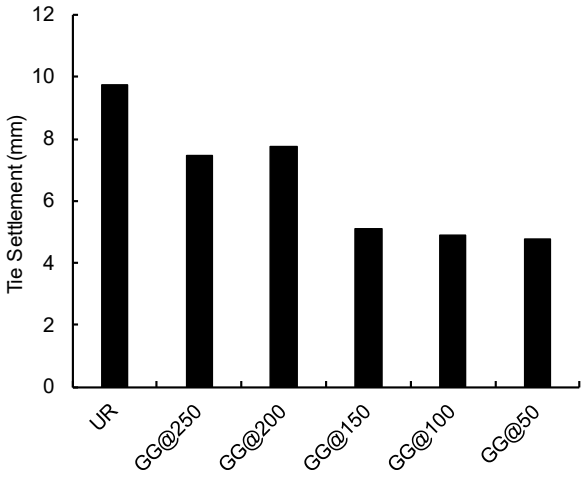

Figure 4. Total tie settlement recorded in unreinforced and geogrid-reinforced ballast layers.

3.2 Particle Displacement

Figure 5 depicts the displacement of ballast particles beneath the tie during the twentieth load cycle, measured in a section of each ballast layer that is cut parallel to their 1,290mm-long side along their center line. Previous observations drawn from Figure 4 demonstrated that geogrids placed at depths of 250mm and 200mm result in similar reductions in tie settlement, while geogrids at 150mm, 100mm, and 50mm lead to notably smaller tie subsidence. As such, Figure 5 shows the particle displacements recorded in the unreinforced (Figure 5a) and reinforced layers with geogrids placed at depths of 250mm, 150mm, and 50mm (Figure 5b, c, and d) for the sake of brevity. Examining the patterns of particle displacement pictured in Figure 5a indicates that the

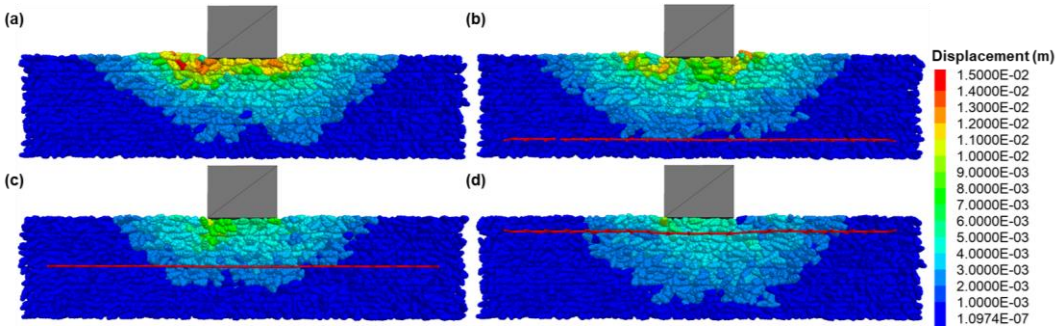

Figure 5. Particle displacement magnitude beneath the tie in (a) the unreinforced ballast layer and in reinforced ballast layers with geogrids placed at depths of (b) 250, (c) 150, and (d) 50mm.

unreinforced ballast bed witnesses the most significant particle movements in response to cyclic loading. Particles displacing the most are located in the immediate vicinity of the tie while the intensity of particle movement progressively wanes as distance away from the loaded area increases. On the other hand, the introduction of geogrids in ballast layers mitigates particle displacement. Figure 5b reveals that the geogrid placed 250mm under the tie decreases the maximum magnitude of particle displacement compared to the unreinforced layer while significant particle movement persists in the ballast bed. However, geogrids situated 150mm and 50mm beneath the tie (Figure 5c and d) appear to be more effective at minimizing particle displacement, both in the extent of the volume of aggregate disturbed by cyclic loading and in the maximum displacement magnitude in each layer.

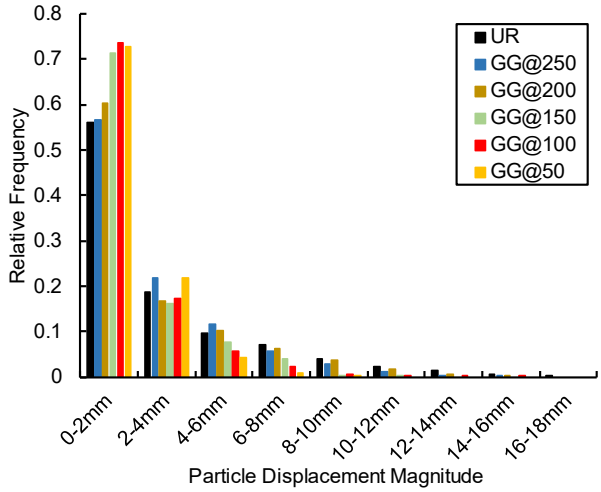

Figure 6. Relative frequency histogram of total particle displacement magnitude at the end of each ballast box test.

Expanding on these insights, Figure 6 presents a relative frequency histogram of total particle displacement across the different ballast layers obtained at the end of each simulation. The histogram echoes the findings drawn from Figure 5 and highlights the superior efficacy of geogrids placed at depths of 150mm or less in curbing particle movement. Indeed, there is a preponderance of particles located in ballast beds with geogrids placed 150mm, 100mm, and 50mm below the tie that experience total displacements of 2mm or less, with each layer having 71.4%, 73.7%, and 72.7% of their particles falling into that category. This contrasts with the unreinforced ballast layer and those with geogrids located 200mm and 250mm under the tie where a respective 55.9%, 60.3%, and 56.7% of particles undergo displacements of 2mm or less. Moreover, as the magnitude of particle displacement increases, the trend reverses with the unreinforced and reinforced layers with geogrids at 200mm and 250mm possessing greater proportions of their particles experiencing large particle movements compared with ballast assemblies with geogrids placed closer to the tie.

From a practical perspective, the findings from Figure 6 not only corroborate the displacement patterns identified in Figure 5 but also elucidate the depth-dependent nature of the geogrid-induced reinforcement observed in Figure 4. Specifically, geogrids placed closer to the tie emerge as more effective in minimizing tie subsidence, with a clear distinction becoming apparent between placement depths of 150mm or less and those exceeding 150mm. This depth-dependence suggests that the reduced tie settlements are, to a certain extent, a consequence of the stabilizing influence of geogrids positioned at depths of 150mm or shallower, which restrict particle displacement more effectively than their deeper-placed counterparts, thereby contributing to the overall structural stability of the ballast layer.

3.3 Particle Contacts

In granular materials such as railroad ballast, loads are transmitted through interparticle contacts that form a contact network. The contact network may be classified into strong and weak interparticle contacts which carry forces greater than or smaller than the average contact force in the granular assembly respectively. Strong forces are the primary contributors to load transmission while weak contact forces provide a structure that supports strong contact force chains. As such, the mechanical behavior and structural stability of a ballast layer are influenced by the packing intensity of its particles. The structure of a ballast layer may be described using a scalar measure of its packing density called the coordination number (CN), which represents the average number of contacts per particle in a granular medium. High coordination numbers have been shown to increase the stability of a granular material, resulting in a greater shear strength and reducing the potential for particle breakage.

To assess the effect of geogrids on the stability of reinforced ballast layers, the coordination number of each

layer considered in this study is computed during the twentieth load cycle and plotted in Figure 7. The lowest coordination number is recorded in the unreinforced ballast assembly with a value of 6.36. Interestingly, the effect of geogrids on the ballast's coordination number bears a resemblance to their effect on the tie settlement and particle displacement and exhibits a similar dependence of the geogrid placement depth. Geogrids located at depths of 200mm and 250mm both generate an increase in CN compared to the unreinforced condition with both layers registering a CN of 6.55. However, geogrids situated at depths of 150mm or less display markedly superior propensities to improve the ballast's packing density compared to geogrids placed at deeper locations. CNs of 6.78, 6.76, and 6.74 are obtained in layers with geogrids 150mm, 100mm, and 50mm under the tie respectively.

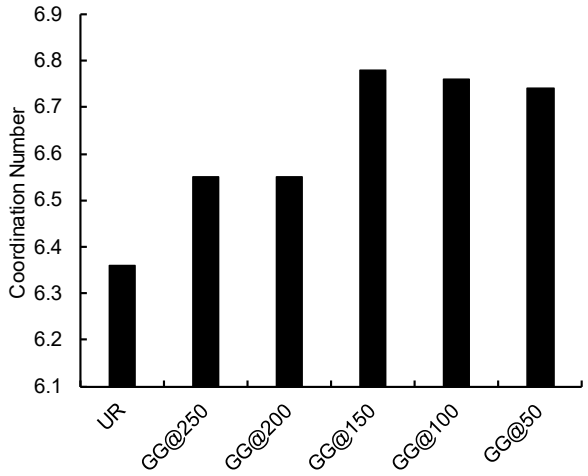

Figure 7. Coordination number in each ballast assembly during the twentieth load cycle.

The increase in CN induced by geogrids produces better-connected ballast assemblies and impacts the load transmission process in the granular layers. This is illustrated by Figure 8 which shows the normalized average strong contact force with depth obtained in the unreinforced and reinforced layers with geogrids placed at depths of 250mm, 150mm, and 50mm recorded during the twentieth load cycle. Average strong contact forces (F) are normalized by being divided by the average strong contact force in the unreinforced ballast bed in the bin stretching from 0 to 50mm ($F_{UR,25}$) above the bottom of the ballast layer. Figure 8 reveals that, in every ballast layer, the average contact force increases as the distance from the loaded area decreases. However, the presence of geogrids and their location within a ballast layer affect the magnitude of contact forces throughout the reinforced granular assemblies. The largest interparticle contact forces are recorded in the unreinforced ballast layer, reaching a maximum $F/F_{UR,25}$ of 1.76 at the layer's top. Geogrid-reinforced layers all display lower average strong contact forces than the unreinforced assembly, with the reduction in contact force being a function of the geogrid placement depth. Geogrids located at depths of 150mm or less result in greater contact force reductions than their deeper-placed counterparts.

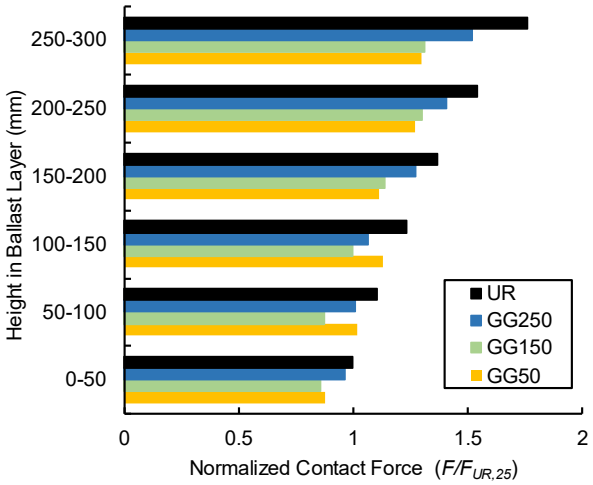

Figure 8. Normalized strong contact forces along the height of the unreinforced and reinforced ballast layers with geogrids at depths of 250mm, 150mm, and 50mm recorded during the twentieth load cycle.

3.4 Energy Dissipation and Geogrid Response

As cyclic loading is applied to a ballast layer, energy is input into the particulate system through the motion of the overlying tie. While a portion of that energy may be stored in the linear springs between contacting clumps, a fraction of it may be dissipated through interparticle sliding that occurs once the frictional strength of a given contact is exceeded. Additionally, energy may be stored in the form of strain energy in the parallel-bonded contacts of geogrids following their deformation in response to the applied loads thereby providing a scalar measure of the load carried by each geogrid. As such, the energy dissipated through frictional slip (E_{Slip}) and the strain energy stored in a geogrid's parallel bond springs (E_{GG}) are tracked during the simulations to dissect the geogrids' impact on energy dissipation in ballast during cyclic loading and shed light on the magnitude of the load carried by each geogrid. Table 1 provides a summary of the total energy dissipated by frictional sliding and each geogrid's bond strain energy recorded during the twentieth load cycle.

Table 1. Slip energy and geogrid parallel bond strain energy in each ballast layer during the twentieth load cycle.

		GG at depth (mm)				
Condition	UR	250	200	150	100	50
E_{slip} (J)	162.3	135.1	139.3	102.2	105.8	107.7
E_{GG} (J)	-	1.1	1.4	1.8	2.3	2.6

*UR: unreinforced, GG: geogrid, E_{slip}: slip energy, E_{GG}: geogrid strain energy

The greatest amount of energy dissipated through interparticle sliding is recorded in the unreinforced ballast assembly, amounting to 162.3J by the end of cyclic loading. This correlates with this ballast layer experiencing the most significant particle displacements (Figure 5), indicating that particle movement is a primary driver of energy dissipation and hence of tie subsidence. As

indicated in Figure 6, the inclusion of geogrids generates appreciable reductions in particle movement, with geogrids placed at shallow depths being more effective at stabilizing ballast. This phenomenon is reflected in the slip energy recorded in geogrid-reinforced layers, as there exists a stark contrast between the reduction in slip energy achieved by geogrids placed at depths exceeding 150mm and those placed at depths of 150mm or less. Geogrids located 200mm and 250mm beneath the tie result in 14.1% and 16.8% reductions in slip energy compared to the unreinforced ballast layer, while their counterparts placed at shallower depths yield an average decrease in energy dissipated through frictional sliding of 35.2%. Similarly, Table 1 points to the fact that as the geogrid placement depth increases, the total strain energy stored in the geogrid's parallel bond springs decreases. The geogrid located 50mm beneath the tie possesses the maximum geogrid strain energy, reaching a value of 2.6J during the twentieth load cycle while the smallest geogrid strain energy of 1.1J is recorded in the geogrid placed at a depth of 250mm. This corroborates the results presented herein, highlighting that a geogrid placed deeper in a ballast layer deforms less than one located at a shallower depth, indicating a reduced ability to stabilize ballast aggregate.

4 CONCLUSIONS

The numerical modeling campaign presented in this paper investigates the impact of geogrids on the behavior of geogrid-reinforced ballast. To do so, a total of six discrete element simulations of ballast box tests conducted on unreinforced and geogrid-reinforced ballast layers are conducted. The simulations, coupled with an analysis that ties observed macroscopic phenomena such as the tie settlement to particle-scale processes such as ballast particle movement and interparticle contacts, offer insights into the behavior of geogrid-reinforced ballast and the effect of the geogrid placement depth. The key findings of this study are summarized below:

- The largest tie settlement occurs in the unreinforced ballast layer. The introduction of geogrids induces reductions in tie settlement that are a function of the geogrid placement depth, with geogrids located at depths of 150mm or less being more effective at minimizing tie settlement than their deeper-placed counterparts
- The application of cyclic loading significantly disturbs a large swath of the ballast particles in the unreinforced ballast layer, with the greatest particle displacements occurring in the vicinity of the load area. Embedding geogrids in ballast mitigates ballast particle displacement, with geogrids located at depths of 150mm or less resulting in the most significant attenuations in particle movement
- The presence of geogrids affects the structure of ballast assemblies by increasing their coordination number. The lowest coordination number occurs in the unreinforced ballast layer, while geogrid-reinforced assemblies exhibit increasing coordination numbers with decreasing geogrid placement depths, indicating that geogrids are conducive to the formation of better-connected granular systems
- Geogrid-induced increases in coordination numbers translate into reductions in average interparticle strong contact forces. Strong interparticle contacts in the unreinforced ballast bed carry the largest average forces while the average force of such contacts progressively decreases in reinforced ballast layers as the geogrid depth becomes smaller
- Less energy is dissipated through frictional slip in geogrid-reinforced layers compared with the unreinforced ballast assembly, with layers reinforced with geogrids placed at shallow depths displaying the most significant decreases in energy dissipation

5 REFERENCES

Bathurst, R. J., & Raymond, G. P. (1987). Geogrid reinforcement of ballasted track. *Transportation Research Record*, *1153*, 8–14.

Brown, S. F., Kwan, J., & Thom, N. H. (2007). Identifying the key parameters that influence geogrid reinforcement of railway ballast. *Geotextiles and Geomembranes*, *25*(6), 326–335. https://doi.org/10.1016/j.geotexmem.2007.06.003

Chen, C., McDowell, G. R., & Thom, N. H. (2012). Discrete element modelling of cyclic loads of geogrid-reinforced ballast under confined and unconfined conditions. *Geotextiles and Geomembranes*, *35*, 76–86. https://doi.org/10.1016/j.geotexmem.2012.07.004

Chrismer, S., & Davis, D. (2000). Cost comparisons of remedial methods to correct track substructure instability. *Transportation Research Record*, *1713*, 10–14. https://doi.org/10.3141/1713-02

Das, B. M. (2016). Use of geogrid in the construction of railroads. *Innovative Infrastructure Solutions*, *1*(1), 15. https://doi.org/10.1007/s41062-016-0017-8

Desbrousses, R. L. E., Meguid, M. A., & Bhat, S. (2021). Effect of Temperature on the Mechanical Properties of Two Polymeric Geogrid Materials. *Geosynthetics International*, 1–31. https://doi.org/10.1680/jgein.21.00032a

Desbrousses, R. L. E., Meguid, M. A., & Bhat, S. (2023). Experimental Investigation of the Effects of Subgrade Strength and Geogrid Location on the Cyclic Response of Geogrid-Reinforced Ballast. *International Journal of Geosynthetics and Ground Engineering*, *9*(6), 67. https://doi.org/10.1007/s40891-023-00486-3

Fernandes, G., Palmeira, E. M., & Gomes, R. C. (2008). Performance of geosynthetic-reinforced alternative sub-ballast material in a railway track. *Geosynthetics International*, *15*(5), 311–321. https://doi.org/10.1680/gein.2008.15.5.311

Hussaini, S. K. K., Indraratna, B., & Vinod, J. S. (2015). Performance assessment of geogrid-reinforced

railroad ballast during cyclic loading. *Transportation Geotechnics*, *2*, 99–107. https://doi.org/10.1016/j.trgeo.2014.11.002

Indraratna, B., Hussaini, S. K. K., & Vinod, J. S. (2013). The lateral displacement response of geogrid-reinforced ballast under cyclic loading. *Geotextiles and Geomembranes*, *39*, 20–29. https://doi.org/10.1016/j.geotexmem.2013.07.007

Itasca. (2022). *Particle Flow Code (PFC3D)* [Computer software].

Jewell, R. A., Milligan, G. W. E., Sarsby, R. W., & Dubois, D. (1984). *Interaction Between Soil and Geogrids.* 18–30.

Kashani, H. F., & Hyslip, J. P. (2018). Ballast Life and Effective Parameters. *2018 Joint Rail Conference*, V001T01A023. https://doi.org/10.1115/JRC2018-6264

Lai, H. J., Zheng, J. J., Zhang, J., Zhang, R. J., & Cui, L. (2014). DEM analysis of "soil"-arching within geogrid-reinforced and unreinforced pile-supported embankments. *Computers and Geotechnics*, *61*, 13–23. https://doi.org/10.1016/j.compgeo.2014.04.007

Li, D., Hyslip, J., Sussmann, T., & Chrismer, S. (2015). *Railway Geotechnics*. CRC Press. https://doi.org/10.1201/b18982

Li, H., & McDowell, G. (2020). Discrete element modelling of two-layered ballast in a box test. *Granular Matter*, *22*(4), 1–14. https://doi.org/10.1007/s10035-020-01046-6

Li, H., & McDowell, G. R. (2018). Discrete element modelling of under sleeper pads using a box test. *Granular Matter*, *20*(2), 1–12. https://doi.org/10.1007/s10035-018-0795-0

McDowell, G. R., & Stickley, P. (2006). Performance of geogrid-reinforced ballast. *Ground Engineering*, *39*(1), 26–30.

Nimbalkar, S., & Indraratna, B. (2016). Improved Performance of Ballasted Rail Track Using Geosynthetics and Rubber Shockmat. *Journal of Geotechnical and Geoenvironmental Engineering*, *142*(8), 04016031. https://doi.org/10.1061/(ASCE)GT.1943-5606.0001491

Qian, Y., Mishra, D., Tutumluer, E., & Kazmee, H. A. (2015). Characterization of geogrid reinforced ballast behavior at different levels of degradation through triaxial shear strength test and discrete element modeling. *Geotextiles and Geomembranes*, *43*(5), 393–402. https://doi.org/10.1016/j.geotexmem.2015.04.012

Sadeghi, J., Tolou Kian, A. R., Khanmoradi, A., & Chopani, M. (2023). Behavior of sand-contaminated ballast reinforced with geogrid under cyclic loading. *Construction and Building Materials*, *362*(August 2022), 129654. https://doi.org/10.1016/j.conbuildmat.2022.129654

Scanlan, K. M. (2018). *Evaluating degraded ballast and track geometry variability along a Canadian freight railroad through ballast maintenance records and ground-penetrating radar* [Ph.D. Thesis]. University of Alberta.

Selig, E. T., & Waters, J. M. (1994). *Track Geotechnology and Substructure Management*. Thomas Telford Ltd.

Sharpe, P., Brough, M. J., & Dixon, J. (2006). Geogrid Trials at Coppull Moor on the West Coast Main Line. *1st International Conference on Railway Foundations–RailFound06*, 367–375. https://www.researchgate.net/publication/288559036

Stahl, M., Konietzky, H., te Kamp, L., & Jas, H. (2014). Discrete element simulation of geogrid-stabilised soil. *Acta Geotechnica*, *9*(6), 1073–1084. https://doi.org/10.1007/s11440-013-0265-0

Suiker, A. S. J., Selig, E. T., & Frenkel, R. (2005). Static and Cyclic Triaxial Testing of Ballast and Subballast. *Journal of Geotechnical and Geoenvironmental Engineering*, *131*(6), 771–782. https://doi.org/10.1061/(ASCE)1090-0241(2005)131:6(771)

Titan Environmental Containment. (2020). *Titan Rail Grid 30* (Issue November, p. 2020).

Transport Canada. (2023). *Rail Jobs*. https://tc.canada.ca/en/corporate-services/jobs-transport-canada/looking-exciting-work-get-job-transportation/rail-jobs